

Internal phase control of fiber laser array based on photodetector array

Kai-Kai Jin(靳凯凯), Jin-Hu Long(龙金虎), Hong-Xiang Chang(常洪祥), Rong-Tao Su(粟荣涛), Jia-Yi Zhang(张嘉怡), Si-Yu Chen(陈思雨), Yan-Xing Ma(马阎星), and Pu Zhou(周朴)

Citation: Chin. Phys. B, 2024, 33 (**7**): 074201. DOI: 10.1088/1674-1056/ad47af
Journal homepage: http://cpb.iphy.ac.cn; http://iopscience.iop.org/cpb

What follows is a list of articles you may be interested in

On the generation of high-quality Nyquist pulses in mode-locked fiber lasers

Yuxuan Ren(任俞宣), Jinman Ge(葛锦蔓), Xiaojun Li(李小军), Junsong Peng(彭俊松), and Heping Zeng(曾和平)
Chin. Phys. B, 2024, 33 (**3**): 034210. DOI: 10.1088/1674-1056/acfa87

Broadband bidirectional Brillouin-Raman random fiber laser with ultra-narrow linewidth

Qian Yang(杨茜), Yang Li(李阳), Hui Zou(邹辉), Jie Mei(梅杰), En-Ming Xu(徐恩明), and Zu-Xing Zhang(张祖兴)
Chin. Phys. B, 2024, 33 (**2**): 024206. DOI: 10.1088/1674-1056/ad09cb

Single-frequency linearly polarized *Q*-switched fiber laser based on Nb_2GeTe_4 saturable absorber

Si-Yu Chen(陈思雨), Hai-Qin Deng(邓海芹), Wan-Ru Zhang(张万儒), Yong-Ping Dai(戴永平), Tao Wang(王涛), Qiang Yu(俞强), Can Li(李灿), Man Jiang(姜曼), Rong-Tao Su(粟荣涛), Jian Wu(吴坚), and Pu Zhou(周朴)
Chin. Phys. B, 2023, 32 (**7**): 074203. DOI: 10.1088/1674-1056/acad6d

Antimonene-based saturable absorber for a soliton mode-locked and *Q*-switched fiber laser in the 2 μm wavelength region

H Ahmad, B Nizamani, M Z Samion, N Yusoff, and M F Ismail
Chin. Phys. B, 2023, 32 (**6**): 064205. DOI: 10.1088/1674-1056/ac891f

High efficiency of Brillouin scattering behavior in single-mode Ge-As-Se-Te fibers at 2 μm

Yue Fu(付悦), Shi-Xun Dai(戴世勋), Lu-Lu Xu(徐路路), Yao-Jun Fang(方耀俊), Ying-Ying Wang(王莹莹), Kai Jiao(焦凯), and Xun-Si Wang(王训四)
Chin. Phys. B, 2023, 32 (**5**): 054206. DOI: 10.1088/1674-1056/ac9a3a

---

Internal phase control of fiber laser array based on photodetector array

Kai-Kai Jin(靳凯凯)[1], Jin-Hu Long(龙金虎)[1], Hong-Xiang Chang(常洪祥)[1], Rong-Tao Su(粟荣涛)[1,2,3,†], Jia-Yi Zhang(张嘉怡)[1], Si-Yu Chen(陈思雨)[1], Yan-Xing Ma(马阎星)[1,2,3], and Pu Zhou(周朴)[1]

[1] *College of Advanced Interdisciplinary Studies, National University of Defense Technology, Changsha* 410073, *China*
[2] *Nanhu Laser Laboratory, National University of Defense Technology, Changsha* 410073, *China*
[3] *Hunan Provincial Key Laboratory of High Energy Laser Technology, National University of Defense Technology, Changsha* 410073, *China*

(Received 14 March 2024; revised manuscript received 5 April 2024; accepted manuscript online 6 May 2024)

Coherent beam combining (CBC) of fiber laser array is a promising technique to realize high output power while maintaining near diffraction-limited beam quality. To implement CBC, an appropriate phase control feedback structure should be established to realize phase-locking. In this paper, an innovative internal active phase control CBC fiber laser array based on photodetector array is proposed. The dynamic phase noises of the laser amplifiers are compensated before being emitted into free space. And the static phase difference compensation of emitting laser array is realized by interference measurement based on photodetector array. The principle of the technique is illustrated and corresponding simulations are carried out, and a CBC system with four laser channels is built to verify the technique. When the phase controllers are turned on, the phase deviation of the laser array is less than $\lambda/20$, and $\sim 95\%$ fringe contrast of the irradiation distribution is obtained. The technique proposed in this paper could provide a reference for the system design of a massive high-power CBC system.

Keywords: fiber laser, laser array, coherent beam combining, internal phase control

PACS: 42.25.Bs, 42.25.Kb, 42.55.Wd, 52.38.–r **DOI:** 10.1088/1674-1056/ad47af

1. Introduction

High-power fiber lasers have been widely used in optical communication, industrial processing, scientific research, and many other fields.[1–8] As a promising technique to realize high output power while maintaining near diffraction-limited beam quality, coherent beam combining (CBC) of fiber laser based on master oscillator power amplifier configuration has drawn many interests in recent years.[9–15] To scale the output power of a CBC system, increased power of single fiber laser amplifier and array expansion are two main ways. However, a single amplifier power improvement is limited by nonlinear effects, thermal effects, and so on.[16–20] Hence, the array number expansion of CBC system is emerging to become an important method for power scaling.

In CBC systems, dynamic noises resulting from environmental and thermal fluctuations always exist, which affect the performance of the phase control and decrease the combining efficiency. Hence, accurate compensation of dynamic noises, especially piston phase noise, is highly required. As an important technique of CBC systems, effective phase control methods have been deeply researched in the past decades, which can be divided into two categories according to the feedback structure of a detected signal. One is the external phase control method, which means that the feedback signals are sampled after fiber laser beamlets output into the free space.[21–26] When increasing the number of tiled combined beams, large-aperture mirrors and lenses are needed to focus the laser array to detect phase noise signals, which would lead to practical difficulties. The other one is the internal phase control method, whose feedback structures are completed before the beamlets are emitted into the free space.[27–30] Based on the internal phase control methods, large-aperture optical elements are not needed and the phase control bandwidth could be further improved by the cascaded control technique.[31]

As an innate disadvantage faced by the internal sensing phase control technique based on spatial structure, static phase difference exists in the system, resulting in the energy inconcentration in the far-field. The static phase difference is caused by the optical path difference among different emitting beamlets in the free space because phase-locking is completed before emitted. In 2021, Long *et al*. used a liquid crystal array to compensate the static phase difference.[28] However, the usage of liquid crystal makes the structure more complex and induces another feedback phase control loop. To meet the challenge in the internal phase control technique, the new phase-locking methods based on photodetector array may be helpful. By controlling the phase of each beamlet to be consistent with the reference beamlet through the photodetector array, the phase-locking process can be completed.[32–35] The arbitrary active phase control of output beamlets has been demonstrated.[36]

In this paper, we propose and experimentally demonstrate

†Corresponding author. E-mail: surongtao@126.com

© 2024 Chinese Physical Society and IOP Publishing Ltd

an innovative internal active phase control technique for a fiber laser array based on spatial structure. The dynamic internal phase noises are detected and compensated based on a spatial structure, which is compatible with a high-power amplifier and easy to expand the combined beamlets. The principle is proposed, and corresponding simulations are carried out as well. An experimental setting with coherently combing four-channel beamlets is built up to prove the technique. The detailed results indicated when the controllers are turned on, the phase deviation of the system is less than $\lambda/20$, and $\sim 95\%$ fringe contrast of the irradiation distribution is obtained.

2. Principle and numerical simulation

Figure 1 shows the schematic drawing of the internal sensing CBC phase control system, taking four beamlets as an example. The seed laser (SL) is preamplified and then split into two channels to form two sub-arrays using a fiber splitter (FS), and each sub-array has two beamlets. In each sub-array, the fiber laser is connected to a 1st phase modulator (1st-PM) and coupled into a pre-amplifier to scale the output power. Then, each sub-array is split into two beamlets by an FS. One of the beamlets is coupled into a 2nd PM, which is employed to compensate the phase difference between the two beamlets. After passing through the amplifiers (AMP) for further power amplification, the beamlets are collimated by the collimators (CO). Following that, most power of the collimated laser is reflected by a small beam splitter (SP) and transmitted into free space to form emitting array via the laser emitting system. Each beamlet is expanded by a beam expander (BE) to obtain a high fill factor in the laser emitting system.

Phase control process can be divided into two steps. The first step is to compensate the dynamic phase noises in the sub-arrays. Collimated beamlets transmit through the small beam splitter, and are focused by the lenses (L) to form far-field interference pattern. The beam array with lower energy is used to generate phase control signals, which is named sampled array. PD1 & PD2 are employed to detect the phase noise signals between the two beamlets in the sub-arrays. When controllers 1 & 2 are in the closed loop, the dynamic phase noises in the subarray are compensated. The second step is to compensate the dynamic phase noises between the two sub-arrays. One of the two beamlets in each sub-array is split by the beam splitter, and then reflected by the plane mirror (M) and converged into PD3 by the lens to form phase control signals. By using controller 3, the relative phase difference between the sub-arrays can be compensated.

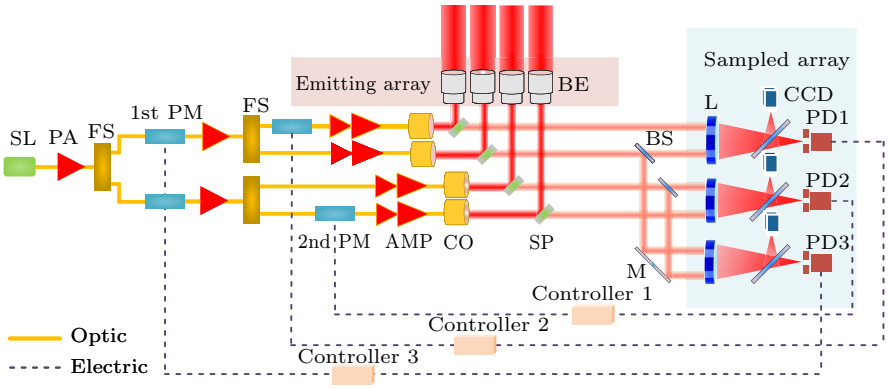


Fig. 1. Schematic drawing of internal sensing phase control system. SL: seed laser; PA: pre-amplifier; FS: fiber splitter; PM: phase modulator; AMP: amplifier; CO: collimator; SP: small beam splitter; BS: beam splitter; M: mirror; L: lens; PD: photodetector; BE: beam expander.

Owing to external static phase differences still existing in the system, the energy distribution in the far-field could not be concentrated in the central main lobe. To meet this challenge, photodetector array could be used to detect and compensate the static phase difference. The principle of the phase difference compensation based on photodetector is shown in Fig. 2, taking two beamlets as an example. There is a static phase difference between the sampled array and the emitted array. Assuming the phase difference between the two emitting beams is $\Delta\varphi$, this means

$$\varphi_{a1} + \varphi_{c1} = \varphi_{a2} + \varphi_{c2} + \Delta\varphi, \tag{1}$$

where φ_{ai} is the dynamic internal phase of the i-th laser chain before the SP, and φ_{ci} is the static external phase of the i-th laser chain between the SP and wavefront of the beam array from the collimators. When the controllers are all turned on, the phases of the sampled array are locked:

$$\varphi_{a1} + \varphi_{b1} = \varphi_{a2} + \varphi_{b2}, \tag{2}$$

where φ_{bi} is the static external phase of the i-th laser chain between the SP and PD. φ_{bi} could be changed by adjusting the position of the PD, as shown in the insert of Fig. 2. When the position of the PD is adjusted, the optical paths of the beams form the lens to the PD are changed. The phase control algorithm will change φ_{ai} to realize phase locking, here we can obtain

$$\varphi'_{a1} + \varphi'_{b1} = \varphi'_{a2} + \varphi'_{b2}, \tag{3}$$

$$\varphi'_{a1} - \varphi'_{a2} = \varphi'_{b2} - \varphi'_{b1} = \Delta\varphi'. \tag{4}$$

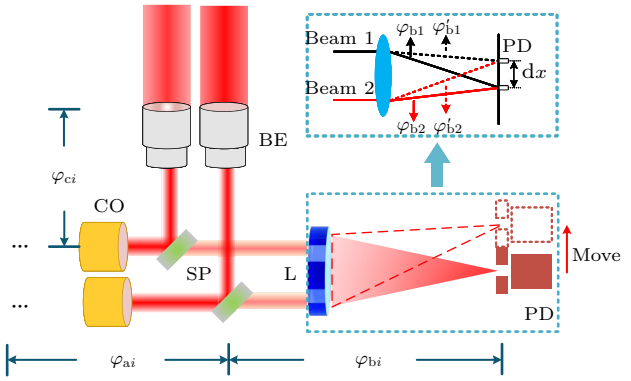


Fig. 2. The schematic drawing of the phase difference compensation based on photodetector.

By adjusting the PD position appropriately to make $\Delta\varphi' = \varphi_{a1} - \varphi_{a2} + \Delta\varphi$, and by substituting Eq. (4) into Eq. (1), we can obtain

$$\varphi'_{a1} + \varphi_{c1} = \varphi'_{a2} + \varphi_{c2}. \tag{5}$$

Hence, the static phase difference between the two emitting beams is compensated.

A simulation of CBC with two beams is carried out. The focal length of the lens is set as 2 m, and the radius of the circular filter in front of PD is 50 μm. The relationship between the phase difference ($\Delta\varphi$) and the center position of the bright fringe can be obtained by assigning different phase differences to the two beamlets. Fill factor F is defined as r/R, where r is the diameter of a beam and R is the distance between the center points of the two beams. The relationship between y and $\Delta\varphi$ is shown in Fig. 3 for $F = 1$, 0.8, and 0.6. It is worth emphasizing that phase mapping is represented by a simple linear function, which means that the static phase noise could be compensated by adjusting the position of bright fringe, which can be realized by moving the PD in the y direction. There are two main factors of the adjustable limitation. The first factor is the system parameter. According to the numerical simulation results shown in Fig. 3, when the fill factor (F) of the laser array is different, the phase shift generated by adjusting the same distance of PD position is also different. For example, when $\Delta\varphi$ changes π, the position of the main lobe in the interference fringe changes by 0.1 mm accordingly when F is 0.6. However, the center position changes by ~ 0.17 mm when F is 1. The second factor is the adjustment accuracy of PD position. The precision of PD position adjustment determines the precision of phase difference compensation. When the adjustment accuracy of the moveable platform reaches 0.01 mm, the phase difference adjustment accuracy can reach $\lambda/1$. When the adjustment precision of the displacement platform is further improved, the precision of phase compensation can also be improved accordingly. In the experiment, the external static phase difference can be compensated by observing far-field interference patter, as shown in Figs. 3(b) and 3(c). When the phase difference is $\pi/2$, the position of PD can be adjusted so that the phase difference is zero.

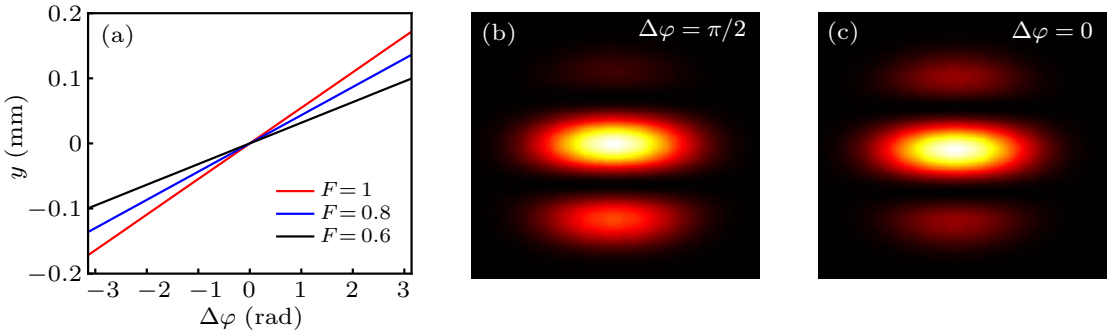


Fig. 3. Simulation results of two beamlets. (a) Fitting curve of the relationship between the phase difference and the center position of the bright fringe, (b) the far-field pattern with $\varphi/2$ phase difference, (c) the far-field pattern with no phase difference.

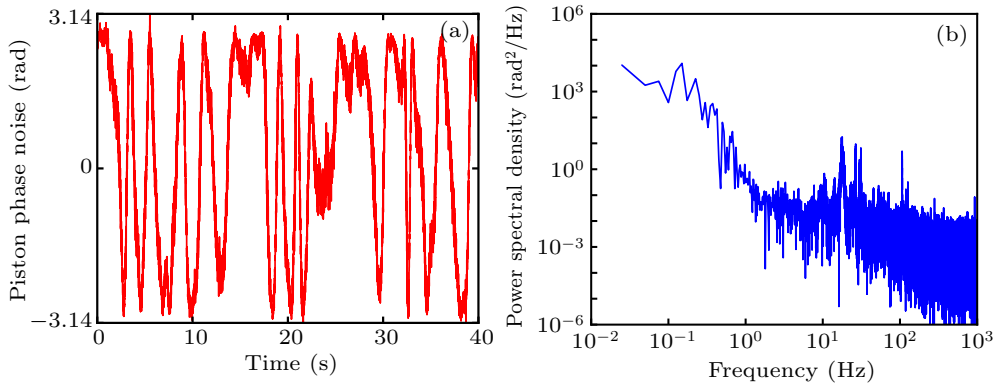


Fig. 4. The piston phase noise characteristics of fiber amplifiers: (a) time domain characteristics, (b) power spectral density.

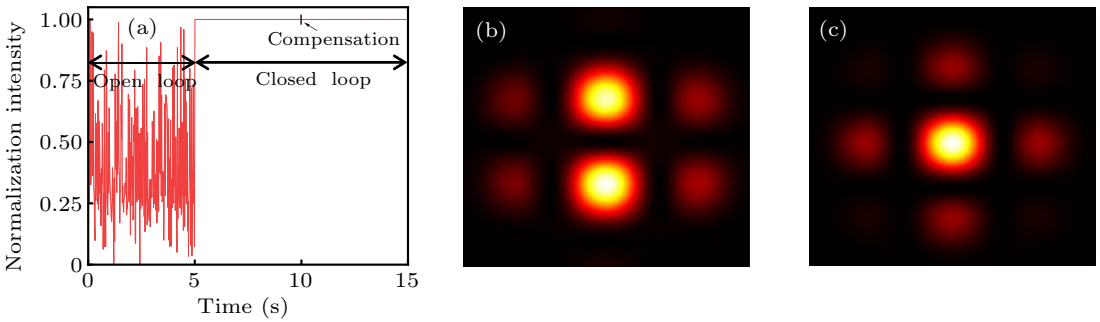


Fig. 5. Simulation results of the system with four beamlets: (a) electrical signal of PD, (b) far-field pattern of emitting array with external phase difference, (c) far-field pattern of emitting array with no external phase difference.

According to the proposed principle, dynamic simulations are carried out. The wavelength is set as 1064 nm. The iteration time of the SPGD algorithm is 500 ns, and the total simulation time in the real world is 15 s. The piston phase noise is injected into the phases of each beamlet. The phase noise is measured from a 50-W fiber amplifier using the coherence detection technique.[37] The total duration of the measurement process is 40 s. The sampling rate is 6.25 kHz. Figure 4 shows the measured phase noise and its power spectral density. The dynamic simulations are shown in Fig. 5. From 0 s to 5 s, the controllers are in the open loop. The controllers are turned on at 5 s, the far-field pattern is shown in Fig. 5(b). Distinct far-field pattern is obtained, but there are phase differences existing. Adjusting the position of PDs at 10 s, the phase difference is compensated as shown in Fig. 5(c).

3. Experimental setup and result

Experimental setting of internal sensing phase control system is shown in Fig. 6. The narrow linewidth seed laser with central wavelength of $\sim$ 1064-nm fiber is connected to a preamplifier and passes through a 1×2 fiber splitter to form two sub-arrays. Subsequently, each sub-array is coupled into a 1st $LiNbO_3$ phase modulator, which is employed to control the phase of the sub-array and realize cascaded phase control. Each sub-array is divided into two beamlets by a beam splitter, one of which is connected to a 2nd $LiNbO_3$ phase modulator, which is employed to compensate the dynamic phase noises in each sub-array. The output beamlets are connected to cascaded fiber amplifiers to scale the output power to be 500 mW. The laser beams from the amplifiers are collimated by four collimators, which are sparsely arranged in square. The diameter of the collimators is 10 mm, and the distance between the adjacent collimators is 40 mm. As for the beam expanders, the diameter of output aperture is 38 mm, and the distance of adjacent beam expanders is 40 mm. Hence, the fill factor of emitted beams is calculated to be 95%.[38] A high fill factor could be obtained by the beam expanders. In the internal phase control process, PD1 & PD2 are used to compensate the internal dynamic phase noises in sub-array, while PD3 is used to compensate the phase noises between the sub-arrays. According to the technique proposed in this paper, the external static phase could be compensated by moving the position of PDs carefully.

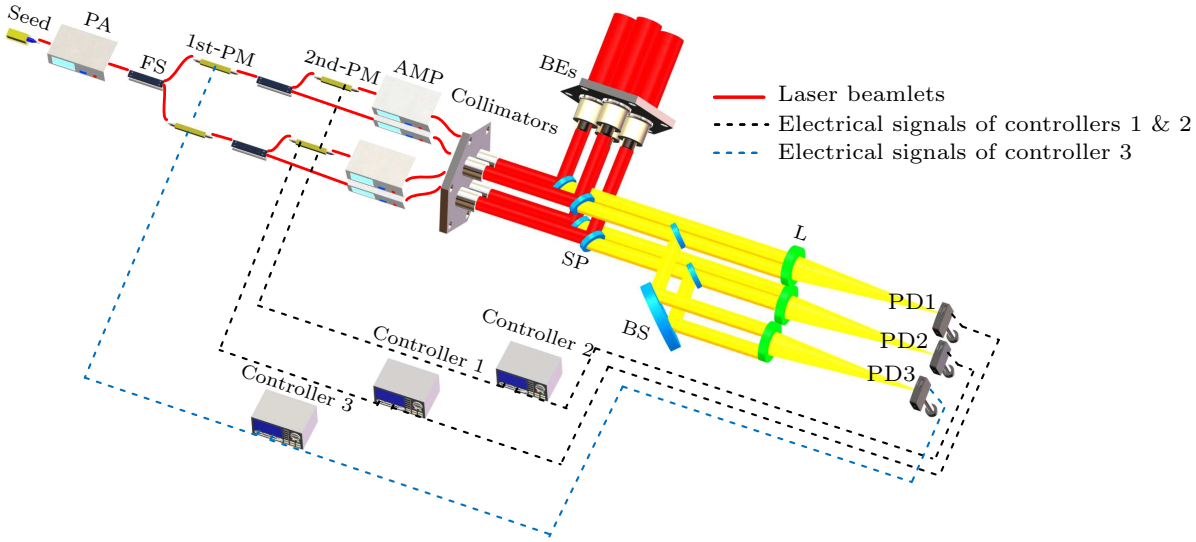


Fig. 6. Experimental setting of internal sensing phase control system.

In the experiment, the phase control process could be observed by the electrical signals from the PDs, as shown in Fig. 7. When the phase controllers are turned off, the electrical signals varied randomly along the time because of dynamic phase noises. The normalized voltage values of the three PDs are about 0.51, 0.54, and 0.46 respectively. In contrast, when the phase controllers are in closed loops and executed the SPGD algorithm simultaneously, the normalized voltage values are locked to be the maximums stably. The values of the three PDs are around 0.91, 0.90, and 0.93 respectively. With the definition of $2\times(V_{\rm rms}/V_{\rm max})^{1/2}$,[39] the phase deviations are less than $\lambda/21$, $\lambda/20$, and $\lambda/28$ respectively, and the time traces for calculating the phase deviations are 8 s. According to the criterion of phase deviation to be less than $\lambda/20$,[40] the dynamic phase noises in the system are compensated effectively.

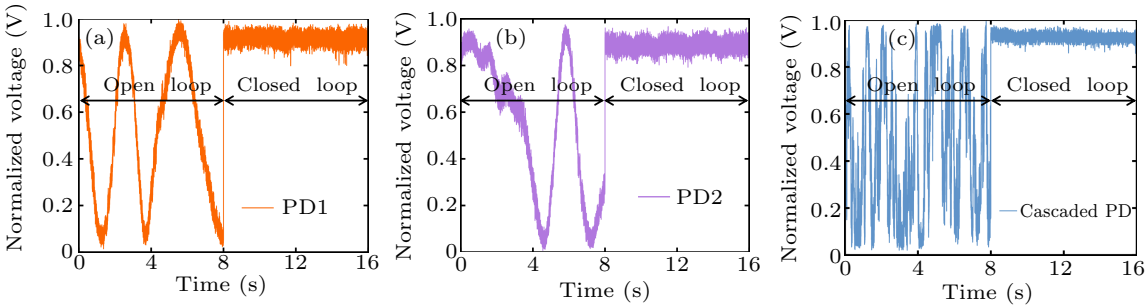


Fig. 7. Electrical signals in open and closed loops from (a) PD1, (b) PD2, and (c) PD3.

To verify the phase control technique based on the phase detector array proposed in this study, the 30-s long-exposure irradiance distributions of sub-array 1 are shown in Fig. 8.

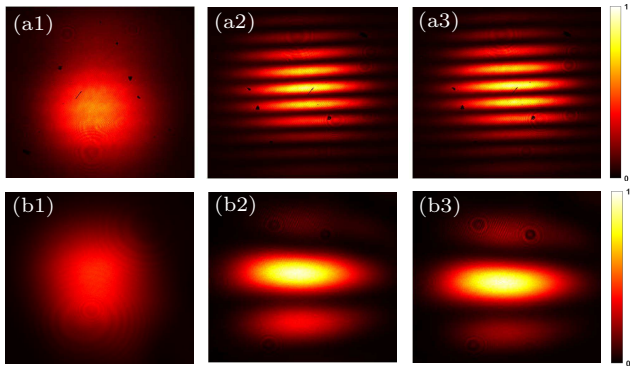


Fig. 8. The sub-array 1 irradiance distribution of (a1) sampled array in an open loop, (a2) sampled array in a closed loop without compensation, (a3) sampled array in a closed loop with compensation, (b1) emitting array in an open loop, (b2) emitting array in a closed loop without compensation, (b3) emitting array in a closed loop with compensation.

One can find that when the controller of sub-array 1 is in an open loop, the irradiance distribution of sampled array and emitting array had low contrast and the energy distribution is dispersed, as shown in Figs. 8(a1) and 8(b1). When the controller is in a closed loop, the dynamic internal phase noises in the sub-array 1 are compensated and the irradiance distribution is distinct and stable, as shown in Figs. 8(a2) and 8(b2). However, one can see that there is a static phase difference between the two beamlets in the far-field interference pattern of emitting array (Fig. 8(b2)), contributing to the energy disperse into the sidelobe. By adjusting the position of PD1 in the phase detector array, the static phase difference could be alleviated as shown in Fig. 8(b3), and the far-field pattern of sampled array after phase compensation is shown in Fig. 8(a3). One can conclude that the phase control technique of the phase detector array could compensate the static phase difference efficiently.

In theory, when the phase of $\Delta\varphi$ is changed by moving PD carefully sampled array, the phase of $\Delta\varphi$ in the emitting array would also be changed accordingly. As for evaluating the fixed phase difference between the two beamlets, the intensity difference between two sub-maximum fringes next to the main maximum fringe can be exploited, as shown in Fig. 9.

The simulation of two-beamlets combination with different phase errors in the sampled array is shown in Fig. 9(a). One can find that the intensity difference of the two sub-maximum changes with the phase difference, and the fitting curve is shown in Fig. 9(b). The experimental optical intensity distribution across cross-sections in sampled array with phase compensated and uncompensated is shown in Fig. 9(c). The normalized intensity difference is 0.088, and the phase changed to 1.22 rad according to the fitting curve. While the phase of the emitting array changed by 1.16 rad calculated from Fig. 9(d). There is a 0.06-rad phase mismatch which might be caused by model error, system parameter error, and adjustment accuracy.

At last, the irradiance distribution of the whole emitting array detected by a CCD is shown in Fig. 10. When the controllers are in an open loop, the phase difference among different emitted beamlets changes severely, and the irradiance distribution is dispersed, as shown in Fig. 10(a). When the controllers are in a closed loop, the internal dynamic phase noises are compensated, stable and distinct fringe could be observed as shown in Fig. 10(b). However, there are external fixed phase differences existed in the emitted array. The external fixed phase difference could be compensated by the detector array technique proposed in this paper, and the adjustment result is shown in Fig. 10(c). The energy distribution

is concentrated in the central main lobe, and the fringe contrast is ∼95% with the definition of $(I_{max}-I_{min})/(I_{max}+I_{min})$, where I_{min} and I_{max} are the adjacent minimum optical intensity and maximum optical intensity on the irradiance distribution pattern. At the phase control accuracy of this experiment, the phase deviation is small, resulting in a high fringe contrast. With the further reduction of the phase deviation, the fringe contrast will increase accordingly.

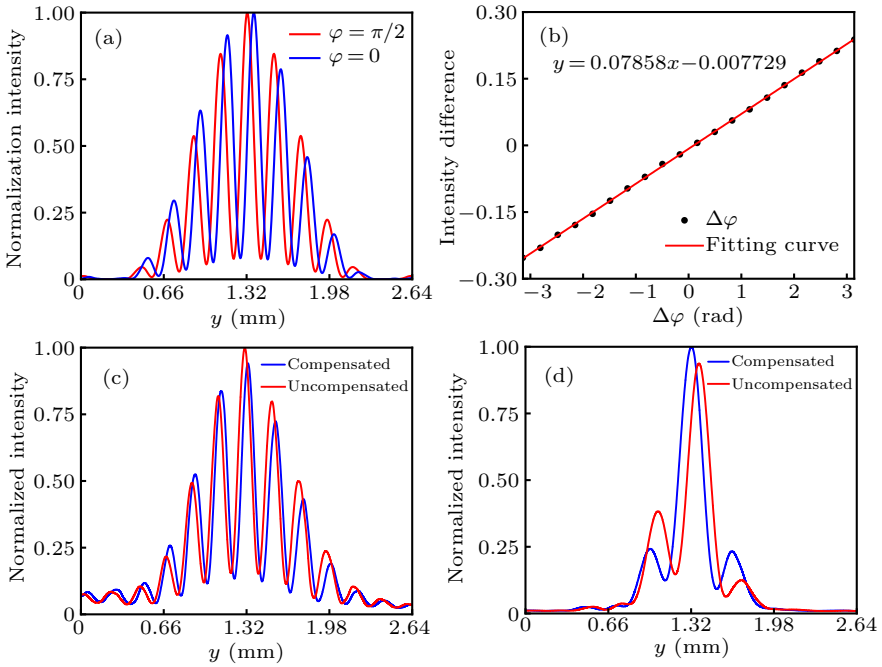


Fig. 9. Analysis of optical intensity distribution across cross-sections. (a) Simulation of two-beamlets combination with different phase errors, (b) fitting curve of the relationship between the phase difference and the intensity difference, (c) experimental optical intensity distribution across cross-sections in sampled array with phase compensated and uncompensated, (d) experimental optical intensity distribution across cross-sections in emitting array with phase compensated and uncompensated.

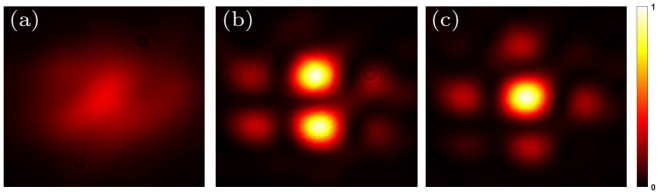


Fig. 10. The 30-s long-exposure irradiance distribution of the emitted array when (a) the controllers are in an open loop, (b) the controllers are in a closed loop without phase compensation, and (c) after phase compensation.

4. Conclusion

In this paper, we proposed an internal phase control technique based on spatial structure. The principle of phase difference compensation is illustrated, and corresponding simulations are carried out. In the experiment, a CBC system is built up to verify the proposed method, which is composed of four fiber beamlets. When all controllers are turned on, the dynamic phase noises in each fiber channel are compensated. Following that, the static phase difference in the system could be compensated by carefully adjusting the position of the photodetector array. The experimental results reveal that the phase deviation is less than $\lambda/20$, stable and distinct irradiation distribution of ∼95% fringe contrast is obtained. The feasibility of the internal phase-locking technique without phase difference is verified. By using the cascaded phase control technique, the bandwidth could be further improved. In addition, the feedback loop of spatial structure in the technique is compatible with the fiber amplifier. This work could provide a reference for the system design of a high-power CBC fiber laser system.

Data availability statement

Data underlying the results presented in this paper are not publicly available at this time but may be obtained from the authors upon reasonable request.

Acknowledgements

Project supported by the National Natural Science Foundation of China (Grant No. 62275272) and the Training Program for Excellent Young Innovators of Changsha (Grant No. KQ2305025).

References

[1] Yang Y, Geng G, Li F, Huang G and Li X Y 2017 *Opt. Express* **25** 27519
[2] Jauregui C, Limpert J and Tünnermann A 2013 *Nat. Photon.* **7** 861
[3] Zervas M N and Codemard C A 2014 *IEEE J. Sel. Top. Quantum Electron.* **20** 219
[4] Mourou G, Brocklesby B, Tajima T and Limpert J 2013 *Nat. Photon.* **7** 258

[5] Shi W, Fang Q, Zhu X, Norwood R A and Peyghambarian N 2014 *Appl. Opt.* **53** 6554
[6] Chen X, Yao T F, Huang L J, An Y, Wu H S, Pan A Y and Zhou P 2023 *Adv. Funct. Mater.* **5** 59
[7] Li J S and Chen Y 2023 *Chin. Phys. B* **32** 124204
[8] Xu X, Huang Y D, Zhang Z L, Liu J L, Lou J, Gao M X, Wu S Y, Fang G Y, Zhao Z X, Chen Y P, Sheng Z M and Chang C. 2023 *Chin. Phys. Lett.* **40** 045201
[9] Yu C X, Augst S J, Redmond S M, Goldizen K C, Murphy D V, Sanchez A and Fan T Y 2011 *Opt. Lett.* **36** 2686
[10] Müller M, Aleshire C, Klenke A, Haddad E, Légaré F, Tünnermann A and Limpert J 2020 *Opt. Lett.* **45** 3083
[11] Fan T Y 2005 *IEEE J. Sel. Top. Quantum Electron.* **11** 567
[12] Yang Y F, Liu H K, Zheng Y, Hu M, Liu C, Qi Y F, He B, Zhou J, Wei Y R and Lou Q H 2014 *Opt. Lett.* **39** 708
[13] Weyrauch T, Vorontsov M, Mangano J, Ovchinnikov V, Bricker D, Polnau E and Rostov A 2016 *Opt. Lett.* **41** 840
[14] Wang X L, Zhou P, Ma Y X, Ma H T, Xu X J, Liu Z J and Zhao Y J 2010 *Chin. Phys. B* **19** 094202
[15] Zheng X R, Ma D N, Jiang G T, Zhang C L and Zhang L L 2023 *Chin. Phys. B* **32** 114210
[16] Smith R G 1972 *Appl. Opt.* **11** 2489
[17] Ke W W, Wang X J, Bao X F and Shu X J 2013 *Opt. Express* **21** 14272
[18] Dawson J W, Messerly M J, Beach R J, Shverdin M Y and Barty C 2008 *Opt. Express* **16** 13240
[19] Zhu J J, Zhou P, Ma Y X, Xu X J and Liu Z J 2011 *Opt. Express* **19** 18645
[20] Jauregui C, Stihler C and Limper J 2020 *Adv. Opt. Photon.* **12** 429
[21] Chosrowjan H, Furuse H, Fujita M, Izawa Y, Kawanaka J, Miyanaga N, Hamamoto K and Yamada T 2013 *Opt. Lett.* **38** 1277
[22] Geng C, Tian Y, Mu J B and Li X Y 2013 *Acta Phys. Sin.* **62** 024206 (in Chinese)
[23] Kermene V, Shpakovych M, Maulion G, Boju A, Armand P, Desfarges-Berthelemot A and Barthelemy A 2021 *Opt. Express* **29** 12307
[24] Wang D, Du Q, Zhou T, Li D and Wilcox R 2021 *Opt. Express* **29** 5694
[25] Shay T M, Benham V, Baker J T, Sanchez A D, Pilkington D and Lu C A 2007 *IEEE J. Sel. Top. Quantum Electron.* **13** 480
[26] Ahn H K and Kong H J 2015 *Opt. Express* **23** 12407
[27] Long J H, Chang H X, Zhang Y Q, Hou T Y, Chang Q, Su R T, Ma Y X, Ma P F and Zhou P 2022 *Opt. Laser Technol.* **148** 107775
[28] Long J H, Hou T Y, Chang Q, Yu T, Su R T, Ma P F, Ma Y X, Zhou P and Si L 2021 *Opt. Lett.* **46** 3665
[29] Chang H X, Su R T, Long J H, Chang Q, Ma P F, Ma Y X and Zhou P 2022 *Opt. Express* **30** 1089
[30] Bowman D J, King M J, Sutton A J, Wuchenich D M, Ward R L, Malikides E A, McClelland D E and Shaddock D A 2013 *Opt. Lett.* **38** 1137
[31] Chang H X, Su R T, Zhang Y Q, Jiang M, Chang Q, Long J H, Ma P F, Ma Y X and Zhou P 2022 *Front. Phys.* **10** 913195
[32] Kabeya D, Kermene V, Fabert M, Benoist J, Desfarges-Berthelemot A and Barthelemy A 2015 *Opt. Express* **23** 031059
[33] Kabeya D, Kermène V, Fabert M, Benoist J, Saucourt J, Desfarges-Berthelemot A and Barthélémy A 2017 *Opt. Express* **25** 1381
[34] Zheng Y, Wang X H, Shen F and Li X Y 2010 *Opt. Express* **18** 26946
[35] Liu Z, Zhi Y S, Zhang M L, Yang L L, Li S, Yan Z Y, Zhang S H, Guo D Y, Li P G, Guo Y F and Tang W H 2022 *Chin. Phys. B* **31** 088503
[36] Zheng Y, Wang X H, Deng L, Shen F and Li X Y 2011 *Appl. Opt.* **50** 2239
[37] Chang Q, Hou T Y, Long J H, Deng Y, Chang H X, Ma P F, Su R T, Ma Y X and Zhou P 2022 *J. Light. Technol.* **40** 6542
[38] Beresnev L A, Andrew Motes R, Townes K J, Marple P, Gurton K, Valenzuela A R, Williamson C, Liu J J and Washer C 2017 *Appl. Opt.* **5** B169
[39] Jolivet V, Bourdon P, Bennal B, Lombard L, Goular D, Pourtal E, Canat G, Jaouen Y, Moreau B and Vasseur O 2009 *IEEE J. Sel. Top. Quantum Electron.* **15** 257
[40] Jones D, Scott A, Clark S, Stace C and Clarke R 2004 *Proc. SPIE* **5335** 125